J Mol Model (2013) 19:1685–1693
DOI 10.1007/s00894-012-1734-3

ORIGINAL PAPER

Theoretical investigation into optical and electronic properties of 1,8-naphthalimide derivatives

Ruifa Jin · Shanshan Tang

Received: 2 September 2012 / Accepted: 13 December 2012 / Published online: 8 January 2013

Abstract A series of 1,8-naphthalimide derivatives has been designed to explore their optical, electronic, and charge transport properties as charge transport and/or luminescent materials for organic light-emitting diodes (OLEDs). The frontier molecular orbitals (FMOs) analysis have shown that the vertical electronic transitions of absorption and emission are characterized as intramolecular charge transfer (ICT) for electron-donating and aromatic groups substituted derivatives. However, the ICT character of the electron-withdrawing substituted derivatives is not significant. The calculated results show that their optical and electronic properties are affected by the substituent groups in 4-position of 1,8-naphthalimide. Our results suggest that 1,8-naphthalimide derivatives with electron-donating $-OCH_3$ and $-N(CH_3)_2$ (**1** and **2**), electron-withdrawing −CN and$-COCH_3$ (**3** and **4**), 2-(thiophen-2-yl)thiophene (**5**), 2,3-dihydrothieno[3,4-b][1, 4] dioxine (**6**), 2-phenyl-1,3,4-oxadiazole (**7**), and benzo[c][1,2,5]thiadiazole (**8**) fragments are expected to be promising candidates for luminescent materials for OLEDs, particularly for **5** and **7**. In addition, **3** and **7** can be used as promising hole transport materials for OLEDs. This study should be helpful in further theoretical investigations on such kind of systems and also to the experimental study for charge transport and/or luminescent materials for OLEDs.

Keywords Charge transport materials · Luminescent materials · 1,8-naphthalimide derivatives · Optical and electronic properties · Organic light-emitting diodes (OLEDs) · Reorganization energy

Introduction

The development of organic light-emitting diodes (OLEDs) materials has received a significant amount of attention in recent years due to their potential applications in the next-generation full-color flat-panel displays [1–4]. The organic electroluminescent devices have shown several advantages over inorganic ones, for example, light weight, potentially low cost, capability of thin-film, large-area, flexible device fabrication, and wide selection of emission colors via molecular design of organic materials. The main obstacle to the application of OLEDs to displays or monitors is still their lower efficiency. The key to increase the efficiency of OLEDs is to design and synthesize efficient fluorescent materials and to balance the charge carrier transport. It is therefore necessary to design and synthesize multifunctional OLEDs materials, which are capable of transporting both holes and electrons in addition to functionalizing as efficient emitters with excellent performance [5, 6]. A number of studies demonstrate the interplay between theory and experiment, which is capable of providing useful insights to the understanding of the nature of molecules [7–9]. The majority of efficient fluorescent materials are obtained with aromatic molecules [10]. Among the various kinds of OLEDs materials, 1,8-naphthalimide derivatives, which are constituted of fused aromatic cycles, include side carbonyl groups, may be considered as the most important building blocks owing to their quite good chemical stability, a large Stokes shift, and high fluorescent quantum yield [11–14]. Moreover, they are also n-type materials and have relatively high electron affinity and excellent transport

Electronic supplementary material The online version of this article (doi:10.1007/s00894-012-1734-3) contains supplementary material, which is available to authorized users.

R. Jin (✉)
College of Chemistry and Chemical Engineering, Chifeng University, Chifeng 024000, China
e-mail: Ruifajin@163.com

S. Tang
College of Resource and Environmental Science, Jilin Agricultural University, Changchun 130118, China

property. Thus, 1,8-naphthalimide derivatives enjoy application in a number of areas including coloration and brightening of polymers [15], potential photosensitive biologically units [16], fluorescent markers in biology [17], light emitting diodes [18–20], fluorescence sensors and switchers [21, 22], laser active media [17], electroluminescent materials [23, 24], and liquid crystal displays [25]. A large variety of auxochromic groups in 1,8-naphthalimide derivatives may be easily grafted to fine tune the absorption and emission wavelengths. Naphthalimides comprise a class of fluorophore whose electronic absorption and emission depend upon the properties of the surrounding medium. The photophysical behavior of 1,8-naphthalimide derivatives is a function of C-4 substitution. The emission spectrum can be tuned by introducing different electron-donating substituent groups, such as N-substituted groups [26], C-substituted groups [27], and O-substituted groups [28], in the 4-position of 1,8-naphthalimide. Furthermore, substitution of electron-donating groups usually increases the intensity of the fluorescence emission, particularly when a methoxy or amino group at C-4 position is used. Recently, a series of novel 1,8-Naphthalimide derivatives (**NIM**), has been reported [29]. Their photophysical property was investigated. It was found that the type of substitutions in C-4 position of naphthalimide very effectively changes the color.

In the present study, our intention was to extend the scope of 1,8-naphthalimides by introducing different electron-donating, electron-withdrawing, or aromatic substituent groups in the 4-position of 1,8-naphthalimides and to describe in more detail their optical property. Furthermore, this structure extended the conjugation systems to favor absorption and emission. An in-depth interpretation of the optical and electronic properties of these compounds has been presented. Several derivatives (**NIM1** and **1**–**8**), as shown in Scheme 1, have been designed to provide a demonstration for the rational design of novel luminescent and charge transporting materials for OLEDs.

Computational details

All calculations have been performed using Gaussian 09 code [30]. Optimizations have been carried out without symmetry constraints. Conventional density functional theory (DFT) methods are well known to differ substantially from ab initio for important classes of molecular properties [31–33]. We take **NIM1** as an example to testify to the validity of the selected approach because it possesses similar constituents with our designed molecules. DFT method was employed to optimize the geometry of **NIM1** in ground states (S_0). The corresponding geometry in the first excited singlet state (S_1) was optimized employing the time dependent-DFT (TD-DFT) method. We selected the B3LYP, PBE0, and B3P86 functionals for all DFT and TD-DFT computations. All geometry optimizations were performed using the 6-31G(d,p) basis set. The main geometrical parameters of **NIM1** in both S_0 and S_1 at the PBE0/6-31G(d,p) and B3P86/6-31G(d,p) levels are similar to those of at B3LYP/6-31G(d,p) level, respectively (see Table SI in Supporting information). Moreover, the reports in literature suggested that B3LYP appeared notably adapted to 1,8-Naphthalimide derivatives [34–38]. In addition, the deviations of the absorption and fluorescent wavelengths for **NIM1** at different levels between calculated results and available experimental data are similar, respectively. Both absorption and fluorescent wavelengths of **NIM1** at TD-B3LYP/6-31+G(d,p) level are in good agreement with the reported experimental observations (see absorption and fluorescent spectra Section). Hence, the geometry

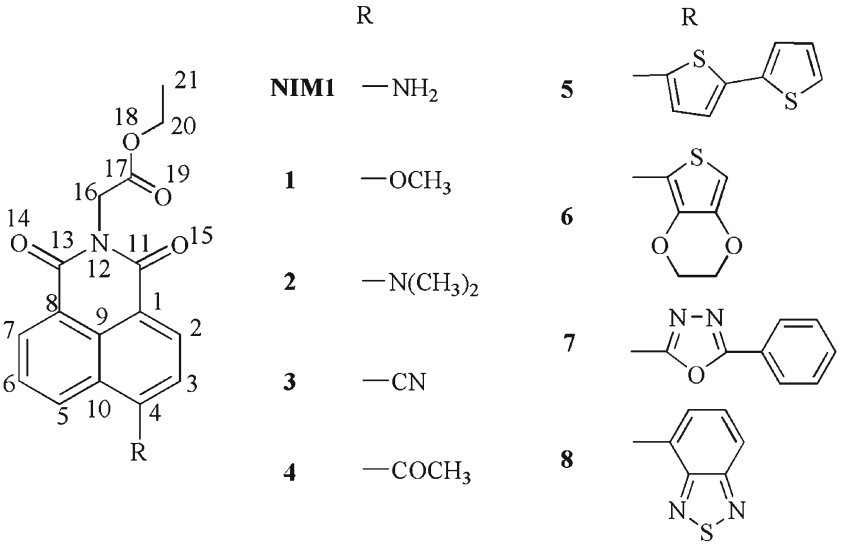

Scheme 1 Geometries of the 1,8-naphthalimide derivatives **MIN1** and **1**–**8**, along with atom numbering

optimization of designed molecules in S_0 were carried out by the B3LYP and PBE0 methods using the 6-31G(d,p) basis set. The corresponding geometry in S_1 were optimized using the TD-B3LYP with 6-31G(d,p) basis set. The harmonic vibrational frequency calculations using the same methods as for the geometry optimizations were used to ascertain the presence of a local minimum. Absorption and fluorescent properties of **NIM1** and **1**–**8** have been predicted using the TD-B3LYP/6-31+G(d,p) method based on the S_0 and S_1 optimized geometries, respectively. To investigate the influence of solvents on the optical properties for the S_0 and S_1 states of the molecular systems in tetrahydrofuran (THF, dielectric constant: 7.58) solvent, we performed the polarized continuum model (PCM) [39] calculations at the TD-DFT level. Moreover, in order to compare with the interested results reported previously [40, 41], the reorganization energies for electron (λ_e) and hole (λ_h) of the molecules were predicted from the single point energy based on the B3LYP/6-31G(d,p) optimized neutral, cationic, and anionic geometries. Generally, the λ can be divided into two parts, external reorganization energy (λ_{ext}) and internal reorganization energy (λ_{int}). λ_{ext} represents the effect of polarized medium on charge transfer; on the other hand, λ_{int} is a measure of structural change between ionic and neutral states [42, 43]. Our designed molecules are used as charge transport materials for OLEDs in the solid film; the dielectric constant of the medium for the molecules is low. The computed values of λ_{ext} in pure organic condensed phases are not only small but also are much smaller than their internal counterparts [44, 45]. Moreover, there is a clear correlation between λ_{int} and charge transfer rate in literature [46, 47]. The reorganization energy could be an important factor that governs the mobility of charge carriers [48]. Therefore, we only pay attention to the discussion of the λ_{int} of the isolated active organic systems due to ignoring any environmental relaxation and changes in this paper. Hence, the reorganization energies for λ_e and λ_h transfer can be calculated by Eqs. 1 and 2 [49]:

$$\lambda e = \left(E_0^- - E_-^-\right) + \left(E_-^0 - E_0^0\right) \quad (1)$$

$$\lambda h = \left(E_0^+ - E_+^+\right) + \left(E_+^0 - E_0^0\right), \quad (2)$$

where $E_0^+\left(E_0^-\right)$ is the energy of the cation (anion) calculated with the optimized structure of the neutral molecule. Similarly, $E_+^+\left(E_-^-\right)$ is the energy of the cation (anion) calculated with the optimized cation (anion) structure, $E_+^0\left(E_-^0\right)$ is the energy of the neutral molecule calculated at the cationic (anionic) state. Finally, E_0^0 is the energy of the neutral molecule in S_0.

The stability is a useful criterion to evaluate the nature of devices for luminescent and transport materials. To predict the stability of **NIM1** and **1**–**8** from a viewpoint of molecular orbital theory, the absolute hardness, η, of **NIM1** and **1**–**8** were calculated using operational definitions [49, 50] given by:

$$\eta = \frac{1}{2}\left(\frac{\partial \mu}{\partial N}\right) = \frac{1}{2}\left(\frac{\partial^2 E}{\partial N^2}\right) = \frac{IP - EA}{2}, \quad (3)$$

where μ is the chemical potential and N is the total electron number. In this work, the values for IP (ionization potential) and EA (electron affinity) were determined according to the equation $IP=E_{cr}-E_p$ and $EA=E_p-E_{ar}$, where p, cr, and ar indicate the parent molecule and the corresponding cation and anion radical generated after electron transfer.

Results and discussion

Molecular structures

The optimized structures of **NIM1** and **1**–**8** in S_0 are plotted in Fig. 1. The main optimized geometric parameters of **NIM1** and **1**–**8** in S_0 and S_1 states are presented in Tables 1 and 2, respectively. The Cartesian coordinates of **NIM1** and **1**–**8** for the S_0 and S_1 are given in Tables SII and SIII in Supporting information, respectively. In the ground state, the comparison of the optimization results for 1,8-naphthalimide moieties of investigated molecules does not reveal any significant change in the geometry of the skeleton. As shown in Table 1, the bond lengths of C_1-C_2, C_2-C_3, C_3-C_4, C_1-C_{11}, C_{11}-N_{12}, C_{11}-O_{15}, and N_{12}-C_{16} in **NIM1** and **1**–**8** are very close to each other and are about 1.38, 1.40, 1.39, 1.48, 1.40, 1.22, and 1.45 Å, respectively. However, the dihedral angles (θ) between 1,8-naphthalimide rings and aromatic substituent groups are different. The values of θ in **5**–**8** are 42.3, 40.4, 1.7, and 124.0°, respectively. The largest value of θ is found in **8**, which is due to the steric hindrances. Comparing the results displayed in Tables 1 and 2, it reveals clearly that electronic excitation leads to the large varieties of the molecules structures. The bond lengths of C_1-C_2, C_3-C_4, and C_{11}-O_{15} in S_1 are shortened, while the corresponding of C_2-C_3, C_1-C_{11}, and C_{11}-N_{12} in S_1 are elongated compared with those in S_0, respectively. However, the bond lengths of C_1-C_{11} in S_1 are similar to those in S_0. The dihedral angles θ in **5**–**8** become larger compared with those in S_0. The dihedral angles between 1,8-naphthalimide rings and the substituent groups of **5** and **6** in S_1 are both almost 90° while the corresponding values of **7** and **8** are about 0 and 140°, respectively.

Frontier molecular orbitals

It is useful to examine the frontier molecular orbitals (FMOs) of the compounds under investigation. The origin

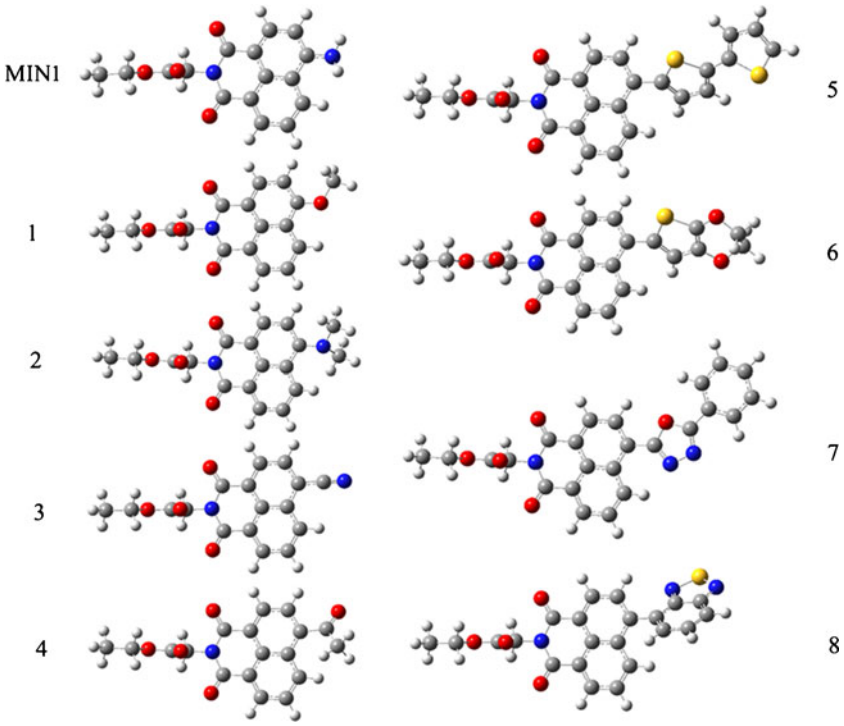

Fig. 1 The optimized structures of **MIN1** and **1**–**8** at the B3LYP/6-31G(d,p) level

of the geometric difference introduced by excitation can be explained, at least in qualitative terms, by analyzing the change in the bonding character of the orbitals involved in the electronic transition for each pair of bonded atoms [51]. An electronic excitation results in some electron density redistribution that affects the molecular geometry [51, 52]. To characterize the optical transitions and the abilities of electron and hole transport, we calculated the distribution patterns of FMOs for **NIM1** and **1**–**8** in S_0 (see Fig. 2). The FMOs energies E_{HOMO} and E_{LUMO}, HOMO–LUMO gaps, and HOMOs and LUMOs contributions (%) of **NIM1** and **1**–**8** using the B3LYP/6-31G(d,p) and PBE0/6-31G(d,p) methods are given in Table 3. As shown in Fig. 2, the $S_0 \rightarrow S_1$ excitation process can be mainly assigned to the HOMO → LUMO transition, which corresponds to a π–π* excited singlet state. For all molecules, both the HOMOs and LUMOs are distributed on the 1,8-naphthalimide and substituent groups moieties. Within TD-B3LYP calculation results, the contributions of the 1,8-naphthalimide moieties for HOMOs in **NIM1** and **1**–**8** are 82.3, 89.5, 66.1, 93.2, 91.7, 23.3, 25.1, 61.2, and 74.6 %, while the corresponding contributions for LUMOs are 96, 97.2, 96.1, 92.7, 88.7, 84.6, 90.5, 82.3 and 21.7 %, respectively. The distribution patterns of the HOMOs and LUMOs also provide a remarkable signature for the charge-transfer character of the vertical $S_0 \rightarrow S_1$ transition. Analysis of the FMOs for **NIM1** and **1**–**8** indicates that the excitation of the electron from the HOMO to LUMO leads the electronic density to flow mainly from the substituent groups moieties to 1,8-naphthalimide moieties except for **3**, **4**, and **8**. The percentages of charge transfer from substituent groups moieties to 1,8-naphthalimide moieties decrease in the order of **6** (65.4 %)>**5** (61.3 %)>**2** (30 %)>**7** (21.1 %)>**NIM1** (13.7 %)>**1** (7.7 %). However, the charge-transfer character of **3** and **4** is not significant. The percentages of charge transfer

Table 1 Main geometrical parameters (bond lengths in Å and dihedral angles in °) of **NIM1** and **1**–**8** in S_0 at the B3LYP/6-31G(d,p) level

Species	C_1-C_2	C_2-C_3	C_3-C_4	C_1-C_{11}	C_{11}-N_{12}	C_{11}-O_{15}	N_{12}-C_{16}	θ(C_3-C_4-R)[a]
NIM1	1.387	1.398	1.395	1.471	1.411	1.225	1.453	
1	1.383	1.407	1.388	1.475	1.408	1.224	1.454	
2	1.383	1.404	1.392	1.475	1.407	1.224	1.453	
3	1.383	1.405	1.389	1.486	1.401	1.222	1.456	
4	1.382	1.404	1.388	1.485	1.402	1.222	1.455	
5	1.383	1.402	1.393	1.480	1.404	1.224	1.454	42.3
6	1.383	1.402	1.394	1.479	1.405	1.224	1.454	40.4
7	1.382	1.402	1.392	1.484	1.401	1.223	1.454	1.7
8	1.382	1.404	1.389	1.482	1.404	1.223	1.454	124.0

[a] θ(C_3-C_4-R): dihedral angles between 1,8-naphthalimide rings and the substituent groups

Table 2 Main geometrical parameters (bond lengths in Å and dihedral angles in °) of **NIM1** and **1**–**8** in S_1 at the TD-B3LYP/6-31G(d,p) level

Species	C_1-C_2	C_2-C_3	C_3-C_4	C_1-C_{11}	C_{11}-N_{12}	C_{11}-O_{15}	N_{12}-C_{16}	θ(C_3-C_4-R)[a]
NIM1	1.404	1.379	1.431	1.488	1.372	1.233	1.451	
1	1.417	1.378	1.428	1.483	1.376	1.234	1.452	
2	1.408	1.384	1.402	1.460	1.403	1.236	1.451	
3	1.421	1.380	1.410	1.414	1.362	1.294	1.464	
4	1.404	1.375	1.434	1.465	1.407	1.230	1.453	
5	1.411	1.383	1.410	1.457	1.409	1.238	1.450	88.8
6	1.411	1.382	1.411	1.457	1.409	1.238	1.450	90.6
7	1.416	1.374	1.431	1.469	1.401	1.232	1.453	0.5
8	1.403	1.385	1.424	1.478	1.404	1.223	1.457	140.3

[a]θ(C_3-C_4-R): dihedral angles between 1,8-naphthalimide rings and the substituent groups

between 1,8-naphthalimide moieties and substituent groups of **3** and **4** are 0.5 and 3 %, respectively. It suggest that the electron-withdrawing groups impose a restriction on the occurrence of the charge-transfer between 1,8-naphthalimide moieties and substituent groups. Interestingly, for **8**, the excitation of the electron from the HOMO to LUMO leads the electronic density to flow mainly from 1,8-naphthalimide moiety to the substituent groups moiety. The percentage of charge transfer of **8** is 52.9 %. From Table 3, one can find that the E_{HOMO} values of **1**–**4**, **7**, and **8** decrease while the corresponding values of **5** and **6** increase compared with that of **NIM1**. However, the values of E_{LUMO} for **1**–**8** decrease compared with those of **NIM1**. The values of HOMO–LUMO gaps E_g for **1**, **3**, and **4** increase while the corresponding values of **2** and **5**–**8** decrease compared with that of **NIM1**. The PBE0 method computed values are similar to those in B3LYP method.

Absorption and fluorescence spectra

The maximum absorption (λ_{abs}) and fluorescence (λ_{fl}) wavelengths of **NIM1** were calculated based on the respective B3LYP/6−31G(d,p) and TD-B3LYP/6−31G(d,p) optimized S_0 and S_1 structures as described above (see Computational details section). To evaluate the influence of the method employed on the simulated values, TD-B3LYP and TD-PBE0 methods have been used. To estimate the basis set, diffuse and polarized functions effect on the calculated results, 6−31G(d), 6−31G(d,p), 6−31+G(d), 6−31+G(d,p), 6−31++G(d), and 6−31++G(d,p) have been used in this case. The results are listed in Table 4 as well as the available experimental data (for comparison). From Table 4, it can be found that both TD-B3LYP and TD-PBE0 methods make agreement with the experiment, TD-B3LYP results show a better agreement than those obtained with TD-PBE0 method for λ_{abs} and λ_{fl} using 6−31+G(d,p). TD-B3LYP calculated λ_{abs} and λ_{fl} showed an improved agreement, deviating by only 17 and 2 nm (with TDB3LYP/6−31+G(d,p)) from its experimental values of 419 and 482 nm, respectively [29]. The corresponding deviations at TD-PBE0/6−31+G(d,p) level are estimated to be 12 and 17 nm, respectively. Within TD-B3LYP calculation results, the influence of the basis set was found to be a little different for these two properties. The addition of polarized functions in the basis set does not significantly affect the λ_{abs} and λ_{fl}. However, the inclusion of diffuse functions to the basis set has a significant effect in the λ_{abs} and λ_{fl}, inclusion of diffuse functions in 6−31G(d) leading to an improvement of 13 and 14 nm on λ_{abs} and λ_{fl}, while with 6−31G(d,p) basis set, the TD-B3LYP computed values increase (by 12 and 16 nm, respectively) when diffuse functions are included. The addition of diffuse function to 6−31+G(d) basis set does not significantly affect the λ_{abs} and λ_{fl}. The λ_{abs} and λ_{fl} values using 6−31+G(d,p) basis set are almost equal to those using 6−31++G(d,p) basis set. Similar trends of λ_{abs} and λ_{fl} are also found in TD-PBE0 computed values. Furthermore, to evaluate the influence of the geometry on the simulated values, the λ_{abs} and λ_{fl} are also calculated based on the respective PBE0/6−31G(d,p) and B3P86/6−31G(d,p) and TD-PBE0/6−31G(d,p) and TD-B3P86/6−31G(d,p) optimized S_0 and S_1 structures (see Tables SIV and SV in Supporting information). It was found that the optimized S_0 and S_1 structures using different methods do not significantly affect the λ_{abs} and λ_{fl}. In all cases, one can find that TD-B3LYP results showed a better agreement with the reported experimental observations [29] than those obtained with TD-PBE0 method. Hence, the λ_{abs} and λ_{fl} of 1,8-Naphthalimide derivatives (**1**–**8**) have been predicted at the TD-B3LYP/6−31+G(d,p)//B3LYP/6−31G(d,p) and TD-B3LYP/6−31+G(d,p)//TD-B3LYP/6−31G(d,p) levels.

The absorption λ_{abs} and fluorescence λ_{fl} wavelengths, main assignments, and the oscillator strength *f* for the most relevant singlet excited states in each molecule are listed in Tables 5 and 6, respectively. The λ_{abs} and λ_{fl} values of **NIM1** are all in agreement with experimental results [29], with the deviations being 17 and 2 nm, respectively. The bathochromic shift between λ_{abs} and λ_{fl} values of **NIM1** is 82 nm, which is comparable to the experimental 63 nm.

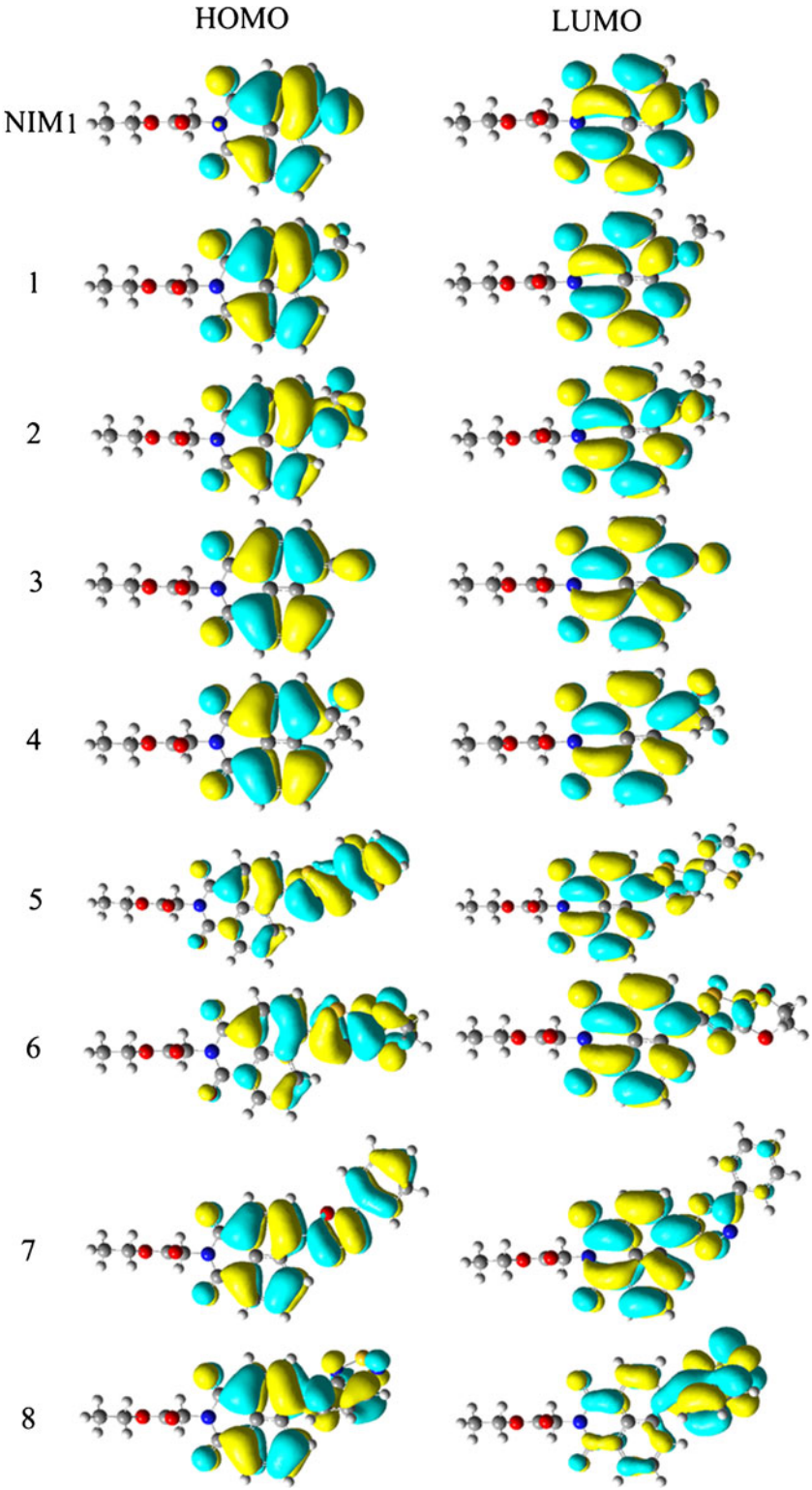

Fig. 2 The FMOs of the investigated molecules at the B3LYP/6-31G(d,p) level

Thus, this result credits to the computational approach, so appropriate electronic transition energies can be predicted at these levels for this kind of system.

For the absorption spectra, the excitation to the S_1 state corresponds mainly to the electron promotion from the HOMO to the LUMO. From Table 5, one can find that the λ_{abs} of **2** and **5**–**8** show bathochromic shifts while **1**, **3**, and **4** show hypsochromic shifts compared with NIM1. The λ_{abs} of 5 and 6 have strong bathochromic shifts 89 and 97 nm, while the λ_{abs} of 2, 7, and 8 show slightly bathochromic

Table 3 The FMOs energies E_{HOMO} and E_{LUMO}, HOMO–LUMO gaps E_g (eV), and HOMOs and LUMOs contributions (%) of **MEBN** and **1**–**8** using the B3LYP/6-31G(d,p) and PBE0/6-31G(d,p) methods

	HOMO			LUMO			
Species	E_{HOMO}	NI[a]	SG[b]	E_{LUMO}	NI	SG	E_g
NIM	−5.776	82.3	17.7	−2.122	96.0	4.0	3.654
	(−5.757)[c]	(88.2)	(17.8)	(−2.090)	(95.9)	(4.10)	(3.667)
1	−6.058	89.5	10.5	−2.158	97.2	2.8	3.900
	(−6.055)	(89.6)	(10.4)	(−2.132)	(97.2)	(2.8)	(3.923)
2	−5.792	66.1	33.9	−2.185	96.1	3.9	3.607
	(−5.772)	(66.7)	(33.3)	(−2.152)	(95.9)	(4.1)	(3.620)
3	−6.917	93.2	6.8	−3.057	92.7	7.3	3.861
	(−6.919)	(93.2)	(6.8)	(−3.035)	(92.7)	(7.3)	(3.884)
4	−6.651	91.7	8.3	−2.810	88.7	11.3	3.841
	(−6.650)	(91.5)	(8.5)	(−2.789)	(88.6)	(11.4)	(3.861)
5	−5.650	23.3	76.7	−2.523	84.6	15.4	3.127
	(5.654)	(23.5)	(76.5)	(−2.489)	(85.2)	(14.8)	(3.156)
6	−5.493	25.1	74.9	−2.390	90.5	9.5	3.103
	(−5.483)	(25.2)	(74.8)	(−2.358)	(90.6)	(9.4)	(3.125)
7	−6.309	61.2	38.8	−2.803	82.3	17.7	3.506
	(−6.296)	(60.7)	(39.3)	(−2.773)	(82.2)	(17.8)	(3.523)
8	−6.253	74.6	25.4	−2.727	21.7	78.3	3.527
	(−6.237)	(73.9)	(26.1)	(−2.689)	(25.5)	(74.5)	(3.548)

[a] *NI* 1,8-naphthalimide moieties

[b] *SG* substituted groups

[c] Data in parenthesis are obtained at the PBE0/6-31G(d) level

shifts 22, 8, and 2 nm compared with that of the parent compound NIM1, respectively. The λ_{abs} values of 1, 3, and 4 show hypsochromic shifts 32, 39, and 29 nm compared with NIM1. Moreover, one can find in Table 5 that 1–8 have larger oscillator strengths than that of NIM1 except the corresponding value of 4 is slightly less than that of NIM1. The oscillator strength for an electronic transition is proportional to the transition moment [53]. In general, larger oscillator strength corresponds to larger experimental

Table 4 The absorption and fluorescence wavelengths and corresponding energies (in parenthesis, in eV) as a function of calculation method and basis set based on the B3LYP/6-31G(d,p) and TD-B3LYP/6−31G(d,p) optimized geometries of **NIM1**

Chemical method	λ_{abs}	λ_{fl}
TD-B3LYP/6−31G(d)	389 (3.18)	468 (2.65)
TD-B3LYP/6−31G(d,p)	390 (3.18)	468 (2.65)
TD-B3LYP/6−31+G(d)	402 (3.08)	484 (2.56)
TD-B3LYP/6−31+G(d,p)	402 (3.08)	484 (2.56)
TD-B3LYP/6−31++G(d)	402 (3.08)	484 (2.56)
TD-B3LYP/6−31++G(d,p)	403 (3.08)	484 (2.56)
TD-PBE0/6−31G(d)	378 (3.28)	453 (2.74)
TD-PBE0/6−31G(d,p)	379 (3.27)	453 (2.74)
TD-PBE0/6−31+G(d)	390 (3.18)	467 (2.66)
TD-PBE0/6−31+G(d,p)	390 (3.18)	467 (2.65)
TD-PBE0/6−31++G(d)	390 (3.18)	467 (2.66)
TD-PBE0/6−31++G(d,p)	390 (3.18)	467 (2.65)
Exp[a]	419	482

[a] Experimental data were taken from ref. [29]

Table 5 The absorption wavelengths λ_{abs} (in nm), the oscillator strength *f*, and main assignments (coefficient) of **NIM1** and **1**–**8** in THF at the TD-B3LYP/6−31+G(d,p)//B3LYP/6−31G(d,p) level, along with available experimental data

Species	λ_{abs}	*f*	Main assignment	Exp[a]
NIM1	402	0.27	H → L (0.70)	419
1	370	0.30	H → L (0.70)	
2	424	0.28	H → L (0.70)	
3	363	0.33	H → L (0.70)	
4	373	0.20	H → L (0.59)	
			H-1 → L (−0.27)	
5	491	0.57	H → L (0.70)	
6	499	0.39	H → L (0.70)	
7	410	0.71	H → L (0.70)	
8	404	0.34	H → L (0.69)	

[a] Experimental data were taken from ref. [29]

absorption coefficient or stronger fluorescence intensity. This indicates that 1–8 shown larger absorption intensity than that of NIM1 except for 4.

For the fluorescence spectra, the fluorescence peaks of NIM1 and 1–8 are mainly correspond to LUMO ← HOMO excitation except the LUMO-1 ← HOMO excitation plays a dominant role for 5 and 6. As shown in from Table 6, the λ_{fl} values of 1–7 show bathochromic shifts 64, 110, 87, 67, 95, 96, and 15, while the corresponding value of 8 show slightly hypsochromic shift 16 nm compared with that of NIM1, respectively. Furthermore, the *f* values 1–8 are larger than that of NIM1 except the corresponding value of 6 is similar to that of NIM1, corresponding to strong fluorescence spectra. This implies that 1–8 have large fluorescent intensity and they are promising luminescent materials for OLEDs, particularly for 5 and 7.

As shown in Tables 5 and 6, it is clear that all the substituent groups can significantly affect the absorption and fluorescence spectra of these molecules. The emission color of molecules can be tuned by the substituent groups. Furthermore, all the substituted derivatives show stronger fluorescence intensity.

Charge transport properties and stability properties

It is well-known that, the lower the reorganization energy values, the higher the charge transfer rate [54, 55]. The calculated reorganization energies for hole and electron are listed in Table 6. The results displayed in Table 6 show that the λ_e values of NIM1 and 1–8 (0.361–0.525 eV) are larger than that of tris(8-hydroxyquinolinato)aluminum(III) (Alq3) (λ_e=0.276 eV), a typical electron transport material [40]. It implies that the electron transfer rates of NIM1 and 1–8 might be lower than that of Alq3. On the other hand, the calculated λ_h values of NIM1 and 1, 2, 4–6, and 8 (0.341–0.636 eV) are larger than that of N,N'-diphenyl-N,N'-bis(3-methlphenyl)-(1,1'-biphenyl)-4,4'-diamine (TPD), which is a typical hole transport material (λ_h=0.290 eV) [41]. However, the λ_h value of 3 (0.202 eV) is smaller than that of TPD, while the corresponding value of 7 (0.295 eV) is almost equal to that of TPD. It indicates that the hole transfer rate of 3 may be higher than that of TPD and the hole transfer rate of 7 may equal to that of TPD. It suggests that 3 and 7 can be used as promising hole transport materials for OLEDs from the stand point of the smaller reorganization energy.

Table 6 The fluorescence wavelengths λ_{flu} (in nm), the oscillator strength *f*, and main assignments (coefficient) of **NIM1** and **1**–**8** in THF at the TD-B3LYP/6−31+G(d,p)//TD-B3LYP/6−31(d,p) level, along with available experimental data

Species	λ_{flu}	*f*	Main assignment	Exp[a]
NIM1	484	0.18	H ← L (0.70)	482
1	420	0.26	H ← L (0.70)	
2	374	0.32	H-1 ← L (0.70)	
3	397	0.34	H ← L (0.70)	
4	417	0.34	H ← L (0.70)	
5	389	1.00	H-1 ← L (0.54)	
			H ← L+1 (−0.45)	
6	388	0.15	H-1 ← L (0.53)	
			H-2 ← L (0.46)	
7	469	0.83	H ← L (0.70)	
8	500	0.27	H ← L (0.69)	

[a] Experimental data were taken from ref. [29]

Table 7 Calculated molecular λ_e, λ_h, and η (all in eV) of **NIM1** and **1**–**8** at the B3LYP/6−31G(d,p) level

Species	λ_h	λ_e	η
NIM1	0.433	0.455	3.208
1	0.354	0.409	3.365
2	0.636	0.433	3.044
3	0.202	0.385	3.381
4	0.340	0.525	3.283
5	0.341	0.393	2.695
6	0.457	0.386	2.780
7	0.295	0.361	2.939
8	0.319	0.386	2.967

The absolute hardness η is the resistance of the chemical potential to change in the number of electrons. As expected, inspection of Table 7 reveals clearly that 1–8 have nearly equal values of absolute hardness, being almost equal to that of NIM1. However, the η values of 5–8 are smaller slightly than the value of NIM1. It indicates that the stabilities of 5–8 are smaller slightly than that of NIM1, which may be due to the steric hindrances. These results reveal that the different substituent groups do not significantly affect the stability of these molecules.

Conclusions

In this paper, a series of 1,8-naphthalimide derivatives has been systematically investigated. The FMOs analysis have shown that the vertical electronic transitions of absorption and emission are characterized as intramolecular charge transfer (ICT) between 1,8-naphthalimide moieties and substituent groups for electron-donating and aromatic groups substituted derivatives. However, the charge-transfer character of the electron-withdrawing substituted derivatives is not significant. The calculated results show that their optical and electronic properties are affected by the substituent groups in 4-position of 1,8-naphthalimide. Furthermore, 1–

8 have large fluorescent intensity. The different substituent groups do not significantly affect the stability of these molecules. Our results suggest that 1–8 are expected to be promising candidates for luminescent materials for OLEDs, particularly for 5 and 7. In addition, 3 and 7 can be used as promising hole transport materials for OLEDs. This study should be helpful in further theoretical investigations on such kind of systems and also to the experimental study for charge transport and/or luminescent materials for OLEDs.

Acknowledgments Financial support from the Natural Science Foundation of Inner Mongolia Autonomous Region (No. 2011ZD02) is gratefully acknowledged.

References

1. Müllen K, Scherf U (2006) Organic light-emitting devices, synthesis, properties, and applications. Wiley-VCH, Weinheim
2. Grimsdale AC, Chan KL, Martin RE, Jokisz PG, Holmes AB (2009) Chem Rev 109:897–1091
3. Dimitrakopoulos CD, Malenfant PRL (2002) Adv Mater 14:99–117
4. Katz HE, Bao ZN, Gilat SL (2001) Acc Chem Res 34:359–369
5. He Z, Wong WY, Yu X, Kwork HS, Lin Z (2006) Inorg Chem 45:10922–10937
6. Slinker J, Bernards D, Houston PL, Abruña HD, Bernhard S, Malliaras GG (2003) Chem Commun 19:2392–2399
7. Liu YL, Feng JK, Ren AM (2008) J Phys Chem A 112:3157–3164
8. Zou LY, Ren AM, Feng JK, Liu YL, Ran XQ, Sun CC (2008) J Phys Chem A 112:12172–12178
9. Tang S, Zhang J (2011) Theor Chem Acc 128:165–174
10. Valeur B (2002) Molecular fluorescence: principles and applications. Wiley-VCH, Weinheim
11. Ramachandram B, Saroja G, Sankaran NB, Samanta A (2000) J Phys Chem B 104:11824–11832
12. Middleton RW, Parrick J, Clarke ED, Wardman P (1986) J Heterocycl Chem 23:849–855
13. Li Y, Xu Y, Qian X, Qu B (2004) Tetrahedron Lett 45:1247–1251
14. Mao P, Qian X, Zhang H, Yao W (2004) Dyes Pigm 60:9–16
15. Bojinov V, Panova I (2007) Dyes Pigm 74:551–560
16. Tao ZF, Qian X (1999) Dyes Pigm 43:139–145
17. Martin E, Weigand R, Pardo A (1996) J Lumin 68:157–164
18. Tian H, Gan J, Chen K, He J, Song Q, Hou X (2002) J Mater Chem 12:1262–1267
19. Grabchev I, Chovelon JM, Qian X (2003) J Photochem Photobiol A Chem 158:37–43
20. Morgado J, Gruner J, Walcott SP, Yong TM, Cervini R, Moratti SC, Holmes AB, Friend RH (1998) Synth Met 95:113–117
21. Grabchev I, Moneva I, Bojinov V, Guittonneau S (2000) J Mater Chem 10:1291–1296
22. Bojinov V, Panova I, Chovelon JM (2008) Sens Actuators B Chem 135:172–180
23. Prezhdo OV, Uspenskii BV, Prezhdo VV, Boszczyk W, Distanov VB (2007) Dyes Pigm 72:42–46
24. Chatterjee S, Pramanik S, Hossain SU, Bhattacharya S, Bhattacharya SC (2007) J Photochem Photobiol A Chem 187:64–71
25. Martynski T, Mykowska K, Bauman D (1994) J Mol Struc 325:161–167
26. Islam A, Cheng CC, Chi SH, Lee SJ, Hela GP, Chen IC, Cheng CH (2005) J Phys Chem B 109:5509–5517
27. Yang JX, Wang XL, Wang XM, Xu LH (2005) Dyes Pigm 66:83–87
28. Magalhaes JL, Pereira RV, Triboni ER, Berci Filho P, Gehlen MH, Nart FC (2006) J Photochem Photobiol A Chem 183:165–170
29. Shakia H, Gharanjig K, Rouhani S, Khosravi A (2010) J Photochem Photobi A Chem 216:44–50
30. Frisch MJT, Trucks GW, Schlegel HB, Scuseria GE, Robb MA, Cheeseman JR, Scalmani G, Barone V, Mennucci B, Petersson GA, Nakatsuji H, Caricato M, Li X, Hratchian HP, Izmaylov AF, Bloino J, Zheng G, Sonnenberg JL, Hada M, Ehara M, Toyota K, Fukuda R, Hasegawa J, Ishida M, Nakajima T, Honda Y, Kitao O, Nakai H, Vreven T, Montgomery JAJ, Peralta JE, Ogliaro F, Bearpark M, Heyd JJ, Brothers E, Kudin KN, Staroverov VN, Kobayashi R, Normand J, Raghavachari K, Rendell A, Burant JC, Iyengar SS, Tomasi J, Cossi M, Rega N, Millam JM, Klene M, Knox JE, Cross JB, Bakken V, Adamo C, Jaramillo J, Gomperts R, Stratmann RE, Yazyev O, Austin AJ, Cammi R, Pomelli C, Ochterski JW, Martin RL, Morokuma K, Zakrzewski VG, Voth GA, Salvador P, Dannenberg JJ, Dapprich S, Daniels AD, Farkas O, Foresman JB, Ortiz JV, Cioslowski J, Fox DJ (2009) Gaussian 09. Gaussian, Wallingford
31. Maroulis G, Karamanis P, Claude Pouchan C (2007) J Chem Phys 126:154316–154321
32. Karamanis P, Pouchan C, Maroulis G (2008) Phys Rev A 77:013201
33. Maroulis G (2008) J Chem Phys 129:044314
34. Mancini G, Zazza C, Aschib M, Sannaa N (2011) Phys Chem Chem Phys 13:2342–2349
35. Li H, Li N, Sun R, Gu H, Ge J, Lu J, Xu Q, Xia X, Wang L (2011) J Phys Chem C 115:8288–8294
36. Dhar S, Roy SS, Rana DK, Bhattacharya S, Bhattacharya S, Bhattacharya SC (2011) J Phys Chem A 115:2216–2224
37. Meng X, Zhu W, Zhang Q, Feng Y, Tan W, Tian H (2008) J Phys Chem B 112:15636–15645
38. Li Z, Yang Q, Chang R, Ma G, Chen M, Zhang W (2011) Dyes Pigm 88:307–314
39. Cornard JP, Lapouge C (2006) J Phys Chem A 110:7159–7166
40. Lin BC, Cheng CP, You ZQ, Hsu CP (2005) J Am Chem Soc 127:66–67
41. Gruhn NE, da Silva Filho DA, Bill TG, Malagoli M, Coropceanu V, Kahn A, Brédas JL (2002) J Am Chem Soc 124:7918–7919
42. Lemaur V, Steel M, Beljonne D, Brédas JL, Cornil J (2005) J Am Chem Soc 127:6077–6086
43. Hutchison GR, Ratner MA, Marks TJ (2005) J Am Chem Soc 127:2339–2350
44. Cheung DL, Troisi A (2010) J Phys Chem C 114:20479–20488
45. McMahon DP, Trois A (2010) J Phys Chem Lett 1:941–946
46. Köse ME, Long H, Kim K, Graf P, Ginley D (2010) J Phys Chem A114:4388–4393
47. Sakanoue K, Motoda M, Sugimoto M, Sakaki S (1999) J Phys Chem A 103:5551–5556
48. Berlin YA, Hutchison GR, Rempala P, Ratner MA, Michl J (2003) J Phys Chem A 107:3970–3980
49. Start MS (1997) J Phys Chem A 101:8296–8301
50. Pearson RG (1985) J Am Chem Soc 107:6801–6806
51. Forés M, Duran M, Solà M, Adamowicz L (1999) J Phys Chem A 103:4413–4420
52. Helal A, Rashid MHO, Choi CH, Kim HS (2011) Tetrahedron 67:2794–2802
53. Schleyer P, Von R, Allinger NL, Clark T, Gasteiger J, Kollman PA, Schaefer HF, III Schreiners PR (1998) Wiley, Chichester, UK
54. Marcus RA (1993) Rev Mod Phys 65:599–610
55. Marcus RA (1964) Annu Rev Phys Chem 15:155–196